

AD A082401

LEVEL II

12  
b.S.

RADC-TR-79-293

In-House Report

November 1979



# STUDY OF THE RADIATION PROPERTIES OF OVERLAPPED, SUBARRAYED SCANNING ANTENNAS

Ronald L. Fante

DTIC  
ELECTE  
S MAR 26 1980 D  
E

APPROVED FOR PUBLIC RELEASE; DISTRIBUTION UNLIMITED

ROME AIR DEVELOPMENT CENTER  
Air Force Systems Command  
Griffiss Air Force Base, New York 13441

80 2 24

This report has been reviewed by the RADC Public Affairs Office (PA) and is releasable to the National Technical Information Service (NTIS). At NTIS it will be releasable to the general public, including foreign nations.

RADC-IR-79-293 has been reviewed and is approved for publication.

APPROVED: *Walter Roiman*  
WALTER ROIMAN, Chief  
Antennas & RF Components Branch

APPROVED: *Alan C. Schell*  
ALAN C. SCHELL, Chief  
Electromagnetic Sciences Division

FOR THE COMMANDER:

*John P. Huss*  
JOHN P. HUSS  
Acting Chief, Plans Office

If your address has changed or if you wish to be removed from the RADC mailing list, or if the addressee is no longer employed by your organization, please notify RADC (FEA), Hanscom AFB MA 01731. This will assist us in maintaining a current mailing list.

Do not return this copy. Retain or destroy.

BEST AVAILABLE COPY

Unclassified

SECURITY CLASSIFICATION OF THIS PAGE (When Data Entered)

REPORT DOCUMENTATION PAGE		READ INSTRUCTIONS BEFORE COMPLETING FORM	
1. REPORT NUMBER RADC-TR-79-293	2. GOVT ACCESSION NO.	3. RECIPIENT'S CATALOG NUMBER	
4. TITLE (and Subtitle) STUDY OF THE RADIATION PROPERTIES OF OVERLAPPED, SUBARRAYED SCANNING ANTENNAS		5. TYPE OF REPORT & PERIOD COVERED In-House Report	
7. AUTHOR(s) Ronald L. Fante		6. PERFORMING ORG. REPORT NUMBER	
8. PERFORMING ORGANIZATION NAME AND ADDRESS Deputy for Electronic Technology (RADC/EEA) Hanscom AFB Massachusetts 01731		9. CONTRACT OR GRANT NUMBER(s)	
11. CONTROLLING OFFICE NAME AND ADDRESS Deputy for Electronic Technology (RADC/EEA) Hanscom AFB Massachusetts 01731		10. PROGRAM ELEMENT, PROJECT, TASK AREA & WORK UNIT NUMBERS 61102F 2305/303	
14. MONITORING AGENCY NAME & ADDRESS (if different from Controlling Office)		12. REPORT DATE Nov 1979	
15. DISTRIBUTION STATEMENT (of this Report) Approved for public release; distribution unlimited.		13. NUMBER OF PAGES 42	
16. SUPPLEMENTARY NOTES		18. SECURITY CLASS. (of this report) Unclassified	
17. KEY WORDS (Continue on reverse side if necessary and identify by block number) Antennas Radiation Scanning Bandwidth		19. DECLASSIFICATION/DOWNGRADING SCHEDULE	
20. ABSTRACT (Continue on reverse side if necessary and identify by block number)  We have studied the properties of an overlapped, subarrayed scanning antenna with emphasis on obtaining low sidelobes and large bandwidths.			

DD FORM 1 JAN 73 1473 EDITION OF 1 NOV 65 IS OBSOLETE

Unclassified

SECURITY CLASSIFICATION OF THIS PAGE (When Data Entered)

309050

Accession For	
NTIS GRA&I	<input checked="checked" type="checkbox"/>
DDC TAB	<input type="checkbox"/>
Unannounced Justification	<input type="checkbox"/>
By _____	
Distribution/	
Availability Codes	
Dist	Avail and/or special
A	

## Contents

1. INTRODUCTION	7
2. PRINCIPLE OF OPERATION	8
3. DISCRETE SYSTEMS	13
4. NUMERICAL RESULTS	14
5. PHASE-ERROR SIDELOBES	23
6. SUMMARY AND DISCUSSION	24
REFERENCES	29
APPENDIX A: Analysis of the General System	31
APPENDIX B: Effect of Subarray Non-Orthogonality	35
APPENDIX C: Sidelobes Due to Phase Errors	39

## Illustrations

1. System Geometry	8
2. Plots of $F(\dots)$ , $G(\dots)$ and $a(\dots)$ at Midband	11
3. Use of $a(\dots)$ to Truncate Sidelobes	13

## Illustrations

4. Effect of Varying $l$ on the Highest Sidelobe of the Radiation Pattern Assuming $2N = 2M = 16$ , $S_0 = 1.5$ , and $\gamma_0 = 0.0525$	16
5. Effect of Varying $l$ on the Second Highest Sidelobe of the Radiation Pattern Assuming $2N = 2M = 16$ , $S_0 = 1.5$ , and $\gamma_0 = 0.0525$	16
6. Illumination on the Flat Face (Face C) of the Lens for $2N = 2M = 16$ , $l = 16$ , $\gamma_0 = 0.0525$ and $R = 1$	17
7. Illumination on the Flat Face of the Lens (Face C) for $2N = 2M = 16$ , $\gamma_0 = 0.0525$ , $l = 20$ and $R = 1$	17
8. Effect of Varying $\gamma_0$ on the Highest Sidelobe of the Radiation Pattern Assuming $2N = 2M = 16$ , $S_0 = 1.5$ and $l = 16.365$	18
9. Effect of Varying $\gamma_0$ on the Second Highest Sidelobe of the Radiation Pattern Assuming $2N = 2M = 16$ , $S_0 = 1.5$ and $l = 16.365$	18
10. A Comparison of the Sidelobe Levels When $a_n = 1$ for All $n$ with Those when $a_n$ is a Cosine Squared Weighting, Assuming $2N = 2M = 16$ , $l = 16.4$ , $\gamma_0 = 0.0525$ and $S_0 = 1.5$	20
11. Non-Orthogonality Loss in the Feed for Uniform and Cosine Squared Illumination on Face B of the Feed Array	20
12. Radiation Pattern for $2N = 2M = 16$ , $l = 16.4$ , $\gamma_0 = 0.0525$ , $S_0 = 1.5$ and $f = 0.85 f_0$	21
13. Radiation Pattern for $2N = 2M = 16$ , $l = 16.4$ , $\gamma_0 = 0.0525$ , $S_0 = 1.5$ and $f = f_0$ ( $R = 1$ )	21
14. Radiation Pattern for $2N = 2M = 16$ , $\gamma_0 = 0.0525$ , $l = 16.4$ , $S_0 = 1.5$ and $f = 1.15 f_0$	22
15. Radiation Pattern for $l = 16.4$ , $2N = 2M = 16$ , $\gamma_0 = 0.0525$ , $S_0 = 1.5$ and $f = 1.25 f_0$	22
16. Main Beam Null Produced by Setting $a_7 = a_8 = 0$ for $2N = 2M = 16$ , $l = 16.4$ , $\gamma_0 = 0.0525$ , $S_0 = 1$ and $R = 1$	25
17. Main Beam Null Produced by Setting $a_7 = a_8 = 0$ , $a_6 = a_9 = 0.5$ , $a_5 = a_{10} = 0.8$ and All Other $a_n = 1$ for $2N = 2M = 16$ , $l = 16.4$ , $\gamma_0 = 0.0525$ , $S_0 = 1.5$ and $R = 1$	26
18. Main Beam Null Produced by Setting $a_7$ , $a_8 = 0$ , $a_6 = a_9 = 0.5$ , $a_5 = a_{10} = 0.8$ and All Other $a_n = 1$ for $2N = 2M = 16$ , $S_0 = 1.5$ , $\gamma_0 = 0.0525$ , $l = 16.4$ and $R = 0.975$	27
19. Radiation Pattern Including Discrete Lens and Near-Field Effects for $2N = 2M = 16$ , $\alpha = 1.833$ , $Q = 0.02864$ , $g = 0.05144$ and $R = 0.85$	33
20. Radiation Pattern Including Discrete Lens and Near-Field Effects for $2N = 2M = 16$ , $\alpha = 1.833$ , $Q = 0.02864$ and $R = 1$	34
21. Radiation Pattern Including Discrete Lens and Near-Field Effects for $2N = 2M = 16$ , $\alpha = 1.833$ , $Q = 0.02864$ , $g = 0.05144$ , and $R = 1.15$	34

## Tables

1. Lens Edge Illumination at Midband for  $2M = 16$ ,  $\gamma_0 = 0.0525$ ,  
 $a_n = 1$  and  $I_p$  Given by (20) 19
2. Error-Sidelobe Coefficients for  $2M = 2N = 16$ ,  $2K = 72$ ,  
 $\alpha = 1.833$ ,  $Q = 0.02164$ ,  $g = 0.05144$  and  $\epsilon = 0.833$  24

## Study of the Radiation Properties of Overlapped, Subarrayed Scanning Antennas

### 1. INTRODUCTION

Radar systems of the future will require wideband electronically steered antennas, with sidelobes below -40 dB. Because the cost of a fully time-delay steered array is excessive, the concept of overlapped subarray (with time delay controlled at the subarray feed input) is attractive. This concept seems to have originated with Rudge and Whithers,<sup>1</sup> and Tang,<sup>2</sup> and recently studied for limited scan by Borgiotti.<sup>3</sup> In this paper we will study the sidelobe and bandwidth properties of this system for large scan angles.

The basic configuration, shown in Figure 1, uses a circular lens fed by a hybrid matrix (with fixed time delays at the matrix output for subarray beam collimation). When an input port on the feed is excited, a distinct subarray distribution is produced on the output face (plane C) of the lens. Therefore different time delays can be applied to each subarray simply by applying different time delays to each input port (in plane A). The main array has phase shifters to produce a phase tilt that scans the subarray patterns.

(Received for publication 15 November 1979)

1. Rudge, A. and Whithers, M. (1971) Proceedings of the IEE (UK) 118:857-863.
2. Tang, R. (1972) Proceedings of 1970 Phased Array Antenna Symposium Artech House, pp. 254-260.
3. Borgiotti, G. (1977) IEEE Transcript on Antennas & Propagation, AP-25: 232-243.

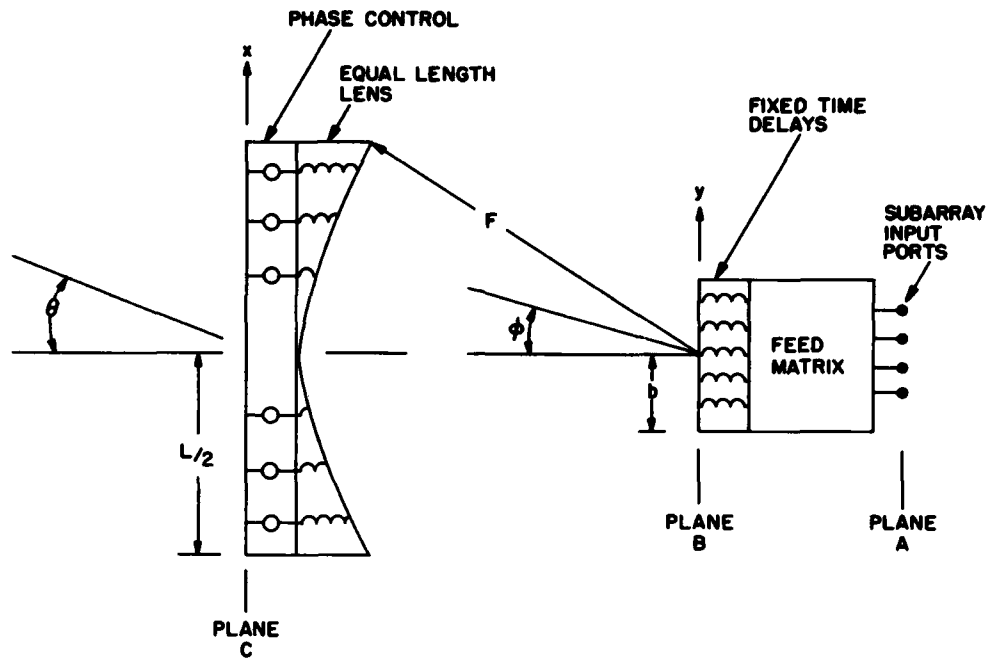


Figure 1. System Geometry

## 2. PRINCIPLE OF OPERATION

Let us first consider the feed array in Figure 1; this can be either a Butler matrix or a true time-delay system, such as a Rotman lens. For the moment we shall approximate the radiating face by a continuous aperture distribution; in the next section this idealization will be removed. If the  $p^{\text{th}}$  input port is excited, the field radiated by the feed at the angle  $u = \sin \phi$  is

$$f_p(u) = \int_{-b}^b dy a(y) e^{iky(u-u_p)}, \quad (1)$$

where  $a(y)$  is the excitation on face B of the feed,  $u_p = \beta \sin \phi$ ,  $\phi_p$  is the angle of the center of the beam produced when the  $p^{\text{th}}$  input port is excited,  $k = 2\pi/\lambda$ ,  $\lambda$  = wavelength and  $\beta$  is defined as



$$\beta = \begin{cases} 1 & \text{True time delay feed} \\ \lambda/\lambda_0 & \text{Butler matrix} \end{cases}$$

where  $\lambda_0$  is the wavelength at midband. In writing (1) we have assumed that the field point (on the lens) lies in the Fraunhofer zone of the feed. The conditions under which this approximation is applicable are discussed in Appendix A.

We next assume that the cylindrical lens shown in Figure 1 has equal line lengths connecting the inner and outer faces. Also we write  $u = \sin \phi = X/F$ ,  $u_p = \beta \sin \phi_p = \beta x_p/F = \beta (p - 1/2) D/F$ , where  $D$  is the separation between the beam centers (and consequently the subarray centers) on the lens, at  $\lambda = \lambda_0$ . Therefore the field distribution at the outer (flat) lens face when only the  $p^{\text{th}}$  port is excited is

$$f_p(x) = b \int_{-1}^1 d\eta a(\eta) e^{i2\pi\gamma R\eta(x/D - \beta p + \beta/2)} \quad (2)$$

where  $\eta = y/b$ ,  $\gamma = bD/\lambda_0 F$  and  $R = \lambda_0/\lambda$ . The result in (2) is the field distribution of the  $p^{\text{th}}$  subarray.

The system in Figure 1 has a large bandwidth because a different time delay,  $T_p$ , is applied to each input port, and consequently to each subarray. When all  $2M$  input ports (subarrays) are excited with a complex amplitude,  $I_p$ , and time delay,  $T_p$ , the total field on the flat face of the lens is

$$f(x) = \sum_{p=-M+1}^M I_p f_p(x) e^{-i\omega T_p} \quad (3)$$

Finally, if we add a linear phase shift  $\exp[-i2\pi x/\lambda_0 \sin \theta_0]$  so as to scan the main beam of the system to the angle  $\theta_0$  we find for the radiated field

$$F(\theta) = \int_{-L/2}^{L/2} dx f(x) \exp \left\{ i \frac{2\pi x}{\lambda_0} (R \sin \theta - \sin \theta_0) \right\} \quad (4)$$

where the aperture distribution  $f(x)$  is given by (3). If we substitute (2) and (3) into (4) and then perform the integration on  $x$  we find

$$F(\theta) = C_1 \sum_{p=-M+1}^M I_p e^{-i\omega T_p} \int_{-1}^1 d\eta a(\eta) \exp[-i2\pi\gamma R\beta\eta(p-1/2)] \cdot \text{sinc}[\pi l(\gamma R\eta + RS - S_0)] \quad (5)$$

where  $S = D/\lambda_0 \sin \theta$ ,  $S_0 = D/\lambda_0 \sin \theta_0$ ,  $C_1$  is a constant and  $l = L/D$ . We next choose

$$\omega T_p = 2\pi \frac{D}{\lambda} (p-1/2) \sin \theta_0 = 2\pi(p-1/2) RS_0 \quad (6)$$

and write  $I_p = \hat{I}_p \exp[i2\pi(p-1/2)S_0]$ . Then (5) becomes

$$F(S) = C_1 \sum_{p=-M+1}^M \hat{I}_p \int_{-1}^1 d\eta a(\eta) \exp\{-i2\pi(p-1/2)[(R-1)S_0 + \gamma R\beta\eta]\} \cdot \text{sinc}[\pi l(\gamma R\eta + RS - S_0)] \quad (7)$$

When  $\pi l \rightarrow \infty$  the principal contribution to the integral in (7) comes from  $\eta = -(RS - S_0)/\gamma R$ . Therefore

$$F(S) \simeq C_2 \sum_{p=-M+1}^M \hat{I}_p \exp\{-i2\pi(p-1/2)[(R-1)S_0 - \beta(RS - S_0)]\} \cdot a\left[-\frac{RS - S_0}{\gamma R}\right] \quad (8)$$

If the feed is a true time-delay system (such as a Rotman lens) so that  $\beta = 1$ , and we also assume  $a(-\eta) = a(\eta)$ , then (8) can be rewritten as

$$F(S) \simeq G[RS - S_0] a\left[\frac{RS - S_0}{\gamma R}\right] \quad (9)$$

$$G[R(S - S_0)] = K \sum_{p=-M+1}^M \hat{I}_p e^{j2\pi(p-1/2)R(S-S_0)} \quad (10)$$

is the radiation pattern corresponding to the input distribution on the feed. Therefore the system radiation pattern is simply the product of the unsquinted feed pattern,  $G[R(S - S_0)]$ , and the (squinted) distribution on face B of the feed array. For example, let us suppose that face B is uniformly weighted, so that  $a(\eta) = 1$  if  $|\eta| \leq 1$  and  $a(\eta) = 0$  for  $|\eta| > 1$ . Then the system radiation pattern at midband is as shown in Figure 2. Note that

$$\gamma < 1 \quad (11)$$

is a necessary condition in order that there be no grating lobes at midband. Unfortunately  $\gamma < 1$  is not always sufficient because when  $l$  is finite the pattern  $a(S)$  has diffraction sidelobes which may be of considerable amplitude at the grating lobe position, as we will see later.

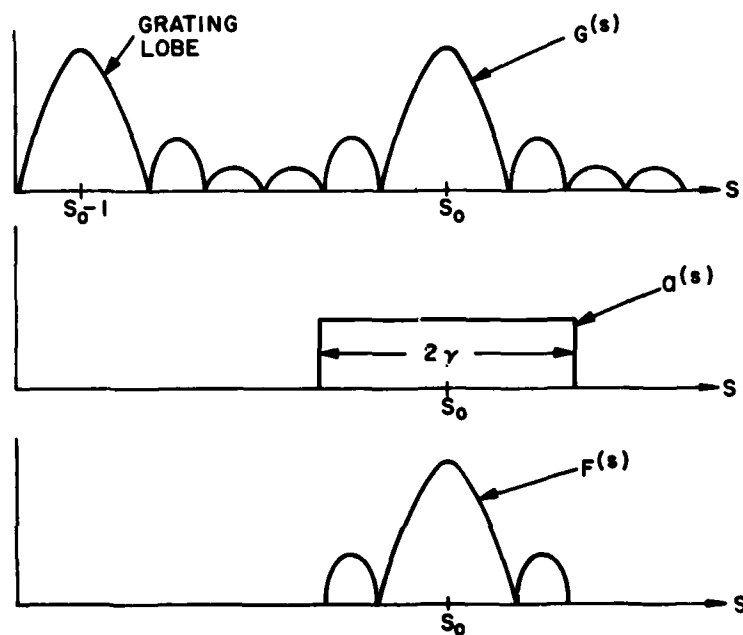


Figure 2. Plots of  $F(\dots)$ ,  $G(\dots)$  and  $a(\dots)$  at Midband

We can estimate the bandwidth of the ideal system by realizing that the grating lobes of  $G[R(S - S_o)]$  occur at  $R(S - S_o) = K$ , where  $K = \pm 1, \pm 2$ , etc. Then because  $a(\eta) = 0$  for  $|\eta| > 1$  it is clear from (9) that there will be no grating lobes if

$$\left| \frac{RS - S_o}{R} \right| > 1 \quad (12)$$

at values of  $S$  such that\*  $R(S - S_o) = K$ , where  $K = \pm 1, \pm 2 \dots$ . By using the aforementioned condition we have found:

i) if  $S_o > 1$  there are no grating lobes if

$$\frac{S_o - 1}{S_o - \gamma} \leq R \leq \frac{S_o + 1}{S_o + \gamma} \quad (13)$$

so that the fractional bandwidth is

$$\text{Fract BW} = \frac{2(1 - \gamma)S_o}{S_o^2 - \gamma^2} \quad (14)$$

ii) if  $S_o < 1$  there are no grating lobes if

$$R < \frac{S_o + 1}{S_o + \gamma} \quad (15)$$

From (13) or (14) it is clear that the fractional bandwidth is largest when  $\gamma = bD/\lambda_o F$  is smallest. Another apparent advantage of designing the system so that  $\gamma$  is small is that we can then use the subarray pattern to cut off the sidelobes of  $G[R(S - S_o)]$  as is shown (at midband in Figure 3). So why don't we do this? There are several reasons: In a real system  $l = L/D$  is not infinite; because  $l$  is finite the sidelobes of  $a(\dots)$  are non-zero and in fact become quite large when  $\gamma l \ll 10$ . In addition, suppose we chose  $2\gamma = B$  (where  $B$  is the null-to-null beamwidth of the main beam), so as to cut off all sidelobes in  $G$  at midband as shown in Figure 3. When the frequency is moved off midband the subarray pattern will truncate a portion of the main beam because  $G(\dots)$  does not squint whereas  $a(\dots)$  does. In fact it is readily shown that a necessary condition for the system to operate at  $R = \lambda_o/\lambda$  without any main beam truncation is that

\*This analysis assumes an infinitesimal grating lobe beamwidth; it is readily extended to finite beamwidths.

$$\gamma > \left| S_0 \left( 1 - \frac{1}{R} \right) \right| + \frac{B}{2R} , \quad (16)$$

where  $B$  is the null-to-null beamwidth of the main beam in  $S$  space.

Therefore we can't make  $\gamma$  arbitrarily small. However, as we shall see later, for a given  $l$  there is actually a value we can choose for  $\gamma$  which is optimum from the standpoint of both low sidelobes and wide bandwidth.\*

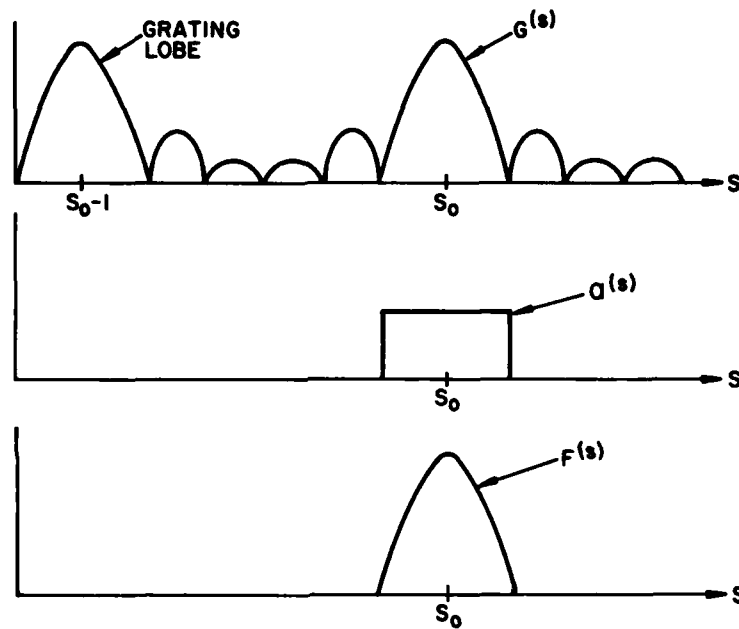


Figure 3. Use of  $a(\dots)$  to Truncate Sidelobes

### 3. DISCRETE SYSTEMS

In a practical system, face B of the feed array will consist of  $2N$  discrete elements, rather than the continuous distribution  $a(\eta)$  assumed in Section 2. Furthermore, the lens (face C) will not be continuous but will also consist of discrete elements, generally spaced slightly less than  $1/2$  wavelength apart. Finally, the lens may not be in the Fraunhofer zone of the feed, and near-field effects must

\* This value of  $\gamma$  is generally such that the subarray beams are non-orthogonal. This gives rise to a system reflection loss, and is discussed in Appendix B.

considered. This general system is analyzed in Appendix A. We show there that the latter two aforementioned effects are generally not significant, so that in the system analysis which follows we will include only the discrete nature of the feed, but will assume, as in Section 2, that the lens is continuous and lies in the far field of the feed system.

If we assume that the feed elements radiate isotropically and have interelement spacing  $\Delta$ , we can replace (1) by

$$f_p(u) = \sum_{n=-N+1}^N a_n \exp \{ ik(n - 1/2)\Delta(u - u_p) \} , \quad (17)$$

where  $a_n$  is the (complex) excitation of the  $n^{\text{th}}$  element on face B. Upon proceeding exactly as we did in the last section we then find that the system radiation pattern  $F(S)$  is given by

$$F(S) = C_3 \sum_{p=-M+1}^M \hat{I}_p \sum_{n=-N+1}^N a_n \exp \{ -i2\pi(p - 1/2)[(R - 1)S_0 + \gamma_0 \beta R(n - 1/2)] \} \\ \cdot \text{sinc} \{ \pi t [RS - S_0 + \gamma_0 R(n - 1/2)] \} , \quad (18)$$

where

$$\gamma_0 = \frac{\Delta D}{\lambda_0 F} . \quad (19)$$

The quantity  $\gamma$  defined in Section 2, is approximately equal to  $N\gamma_0$ .

#### 4. NUMERICAL RESULTS

We shall study (18) for the case when

$$\hat{I}_p = 1 + \left[ \frac{\cos(\pi/M)}{\cos(\pi/2M)} \right] \cos \left[ \frac{\pi}{M} (p - 1/2) \right] . \quad (20)$$

In this case the summation on  $p$  is readily performed and (18) becomes

$$F(S) = C_4 \sum_{j=1}^{2N} a_{j-N} \text{sinc} \{ \pi l [RS - S_0 + \gamma_0 R(j - N - 1/2)] \} \\ \cdot \frac{\sin M\Phi}{2M \sin(\Phi/2)} \frac{\cos \Phi \left[ 1 - \cos \frac{\pi}{M} \right]}{\cos \Phi - \cos \left( \frac{\pi}{M} \right)} \quad (21)$$

where

$$\Phi = 2\pi[(R - 1)S_0 + \gamma_0 R\beta(j - N - 1/2)] \quad (22)$$

and  $C_4$  is a constant. We have evaluated (21) for numerous cases. We first performed a parametric study of the effect on the radiation pattern of varying  $\gamma_0$  and  $l$ . In Figures 4 and 5 we show\* the effects on the two highest sidelobe levels when  $l = L/D$  is varied but  $\gamma_0 = \Delta D/\lambda_0 F$  is held fixed. We note that the sidelobes are relatively insensitive to the value of  $l$  and are lowest when  $l$  is of order  $2M$ , the number of subarray beams. This behavior is readily understood by calculating the total lens illumination

$$f(x) = \sum_{p=-M+1}^M I_p f_p(x) e^{-i\omega T_p} \quad (23)$$

We find that the edge illumination on the lens is smallest for  $l$  slightly greater than  $2M$ , as is clear from Table 1. Typical aperture illuminations are shown in Figures 6 and 7 for  $l = 16$  and  $20$ , respectively. Obviously, the illumination for  $l = 16$  is preferable to that for  $l = 20$ , because there are then no nulls in the aperture distribution.

In Figures 8 and 9 we show the effect of varying  $\gamma_0 = \Delta D/\lambda_0 F$  when  $l$  is held fixed. We note that the sidelobe levels are rather sensitive to the value chosen for  $\gamma_0$ , and if we desire that all sidelobes (except the first) be well below  $-40$  dB over a 30 percent band ( $f_0 \pm 0.15 f_0$ ) we should choose  $0.050 \leq \gamma_0 \leq 0.06$  for the case when  $l = 16.365$  and  $2M = 16$ . By plotting sidelobe levels for a number of different values of  $l$  and  $M$  we have found that  $\gamma_0$  should be chosen approximately equal to  $(0.85/2M)$ .

\*In all the results which follow it is assumed that the feed is a true time-delay system, so  $\beta = 1$ .

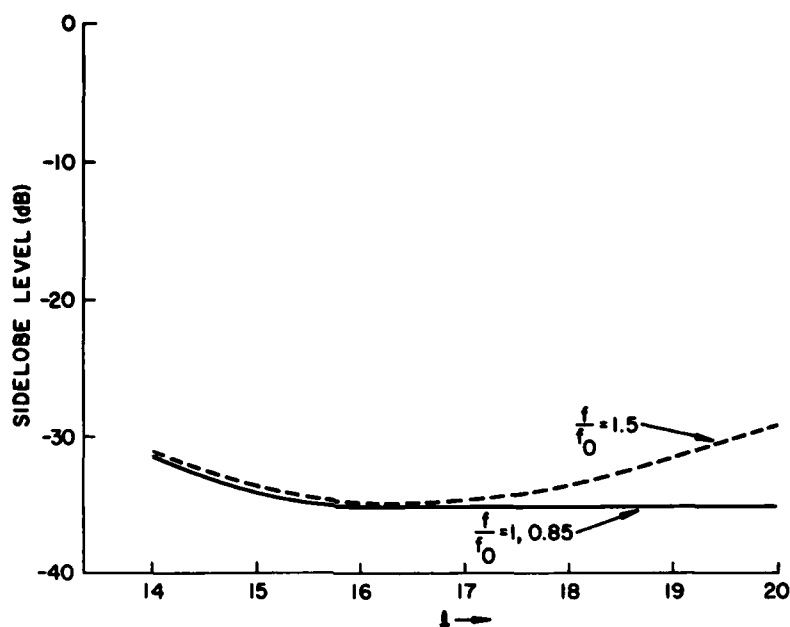


Figure 4. Effect of Varying  $l$  on the Highest Sidelobe of the Radiation Pattern Assuming  $2N = 2M = 16$ ,  $S_0 = 1.5$ , and  $\gamma_0 = 0.0525$

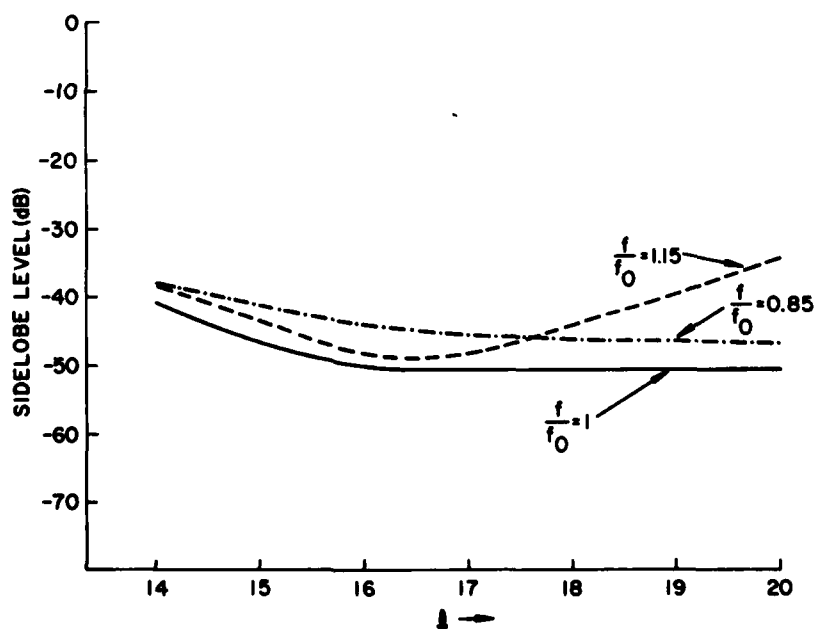


Figure 5. Effect of Varying  $l$  on the Second Highest Sidelobe of the Radiation Pattern Assuming  $2N = 2M = 16$ ,  $S_0 = 1.5$ , and  $\gamma_0 = 0.0525$



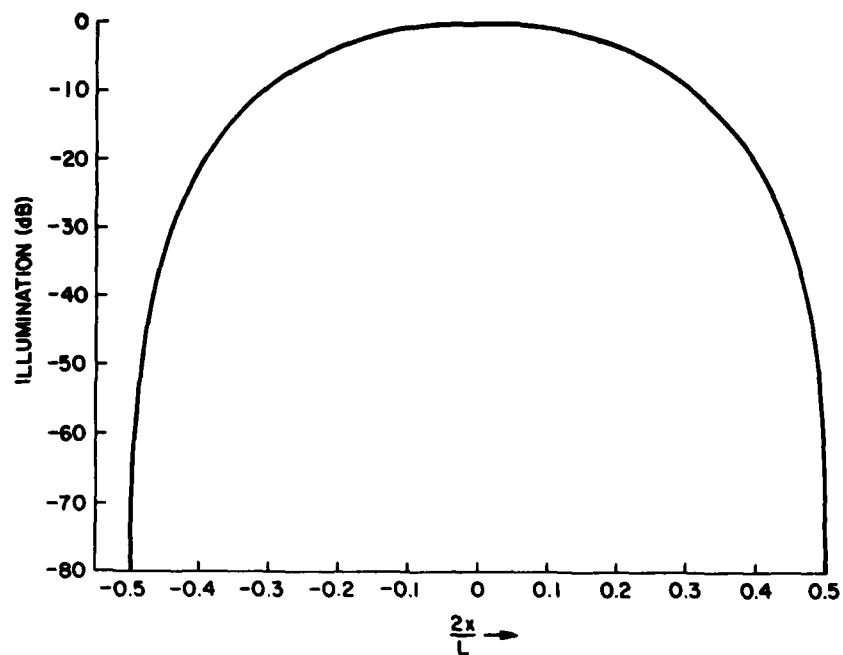


Figure 6. Illumination on the Flat Face (Face C) of the Lens for  $2N = 2M = 16$ ,  $l = 16$ ,  $\gamma_0 = 0.0525$  and  $R = 1$

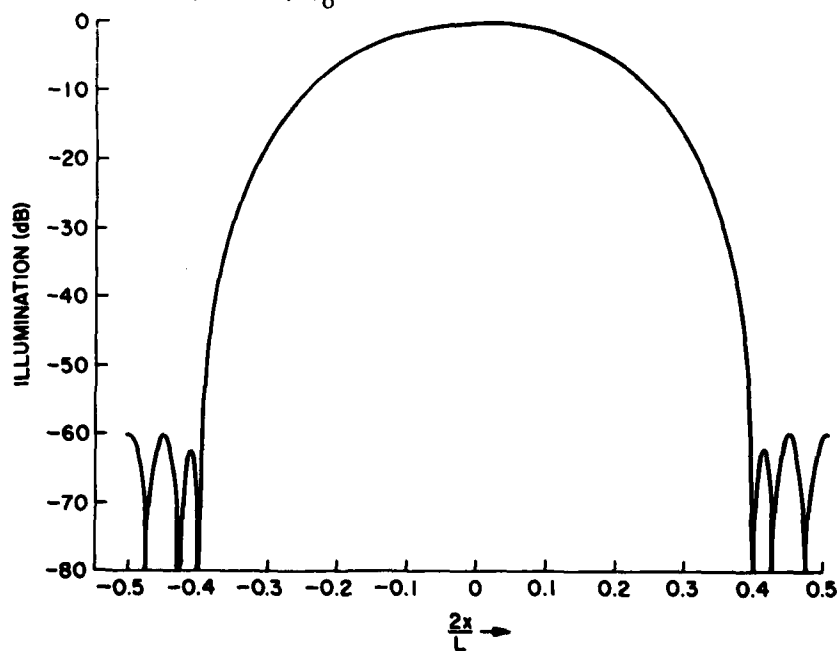


Figure 7. Illumination on the Flat Face of the Lens (Face C) for  $2N = 2M = 16$ ,  $\gamma_0 = 0.0525$ ,  $l = 20$  and  $R = 1$

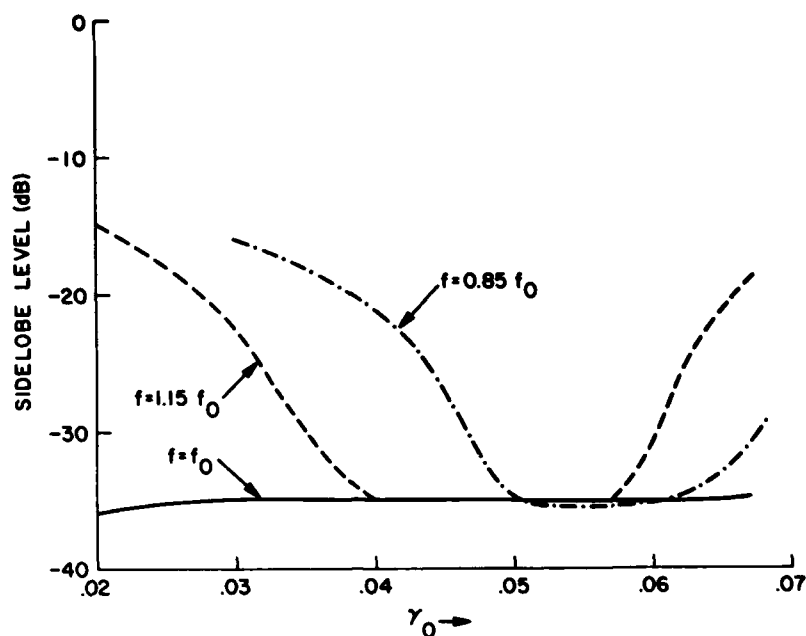


Figure 8. Effect of Varying  $\gamma_0$  on the Highest Sidelobe of the Radiation Pattern Assuming  $2N = 2M = 16$ ,  $S_0 = 1.5$  and  $l = 16.365$

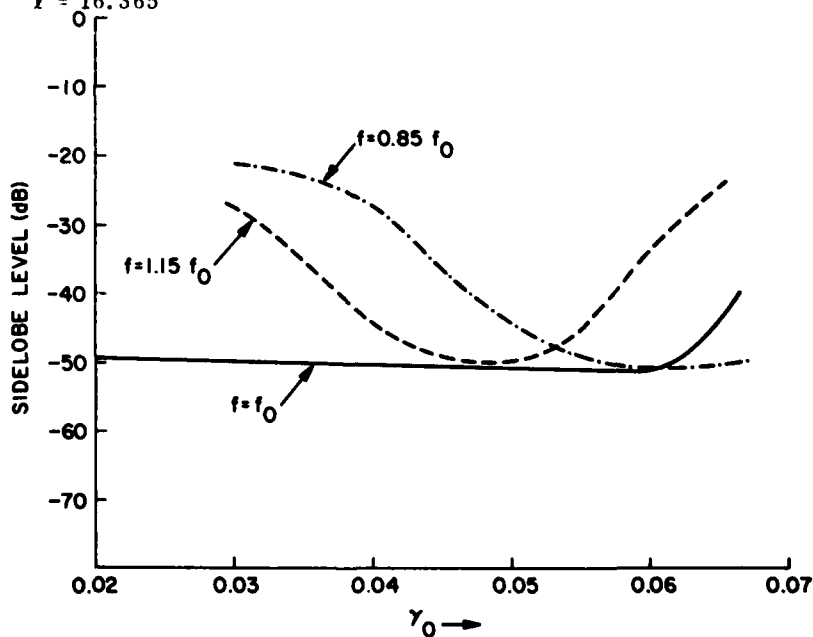


Figure 9. Effect of Varying  $\gamma_0$  on the Second Highest Sidelobe of the Radiation Pattern Assuming  $2N = 2M = 16$ ,  $S_0 = 1.5$  and  $l = 16.365$

Table 1. Lens Edge Illumination at Midband for  $2M = 16$ ,  $\gamma_0 = 0.0525$ ,  $a_n = 1$  and  $I_p$  given by (20)

$l$	Edge Illumination (dB)
10	-10.2
12	-16.6
14	-28.6
15	-40.1
15.5	-50.0
16	-95.7
16.5	-62.5
17	-73.9
17.5	-64.3
18	-59.9
20	-59.9

In Figure 10 we show the amplitude of the two highest sidelobes when  $l = 16.4$  and  $\gamma_0 = 0.0525$  and the beam is scanned to  $\sin \theta_0 = 1.5 \lambda_0/D$  (that is,  $S_0 = 3/2$ ). Shown on Figure 10 are the sidelobe levels for both a uniform illumination,  $a_n = 1$ , and a cosine squared illumination on face B of the feed array. The purpose of comparing these two cases is because Mailloux<sup>4</sup> has suggested that a cosine squared illumination,  $a_n$ , might give lower sidelobes than the uniform illumination. As we can see from Figure 10, this is true near midband, but over a wide bandwidth the uniform illumination on face B actually gives better sidelobe performance. Another disadvantage of using a cosine squared (or other tapered illumination) on face B is that, even at midband, this illumination produces non-orthogonal sub-arrays, and this leads to a reflection loss at the feed input. This problem has been studied in Appendix B and the results plotted in Figure 11. We note from Figure 11 that when  $\gamma_0 = 0.0625$  (that is,  $2\pi N\gamma_0 = 2\pi$ ) there is no orthogonality loss for the uniform illumination, whereas the cosine squared illumination on face B suffers more than a 4 dB reflection loss because of non-orthogonality. Therefore for the parameters chosen there appears to be no advantage to using a tapered distribution on face B, and  $a_n = 1$  (for all  $n$ ) appears to be the preferable illumination.

In Figures 12 to 15 we show the actual radiation patterns for the case of a beam scanned to  $S_0 = (D/\lambda_0) \sin \theta_0 = 1.5$  for the different relative frequencies

4. Mailloux, R. (1979) Digest of 1979 IEEE International Antennas and Propagation Symposium, Seattle, Washington, pp 30-33.

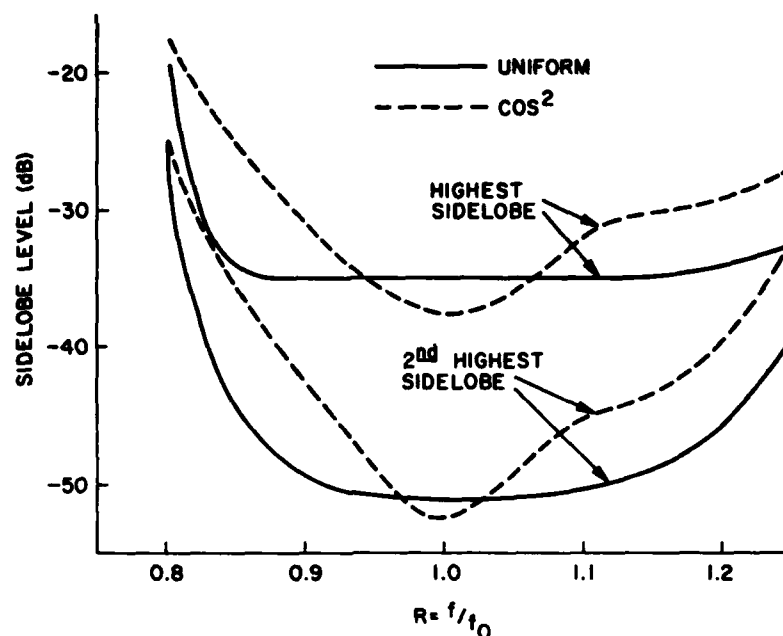


Figure 10. A Comparison of the Sidelobe Levels When  $a_n = 1$  for All  $n$  with Those when  $a_n$  is a Cosine Squared Weighting, Assuming  $2N = 2M = 16$ ,  $l = 16.4$ ,  $\gamma_0 = 0.0525$  and  $S_0 = 1.5$

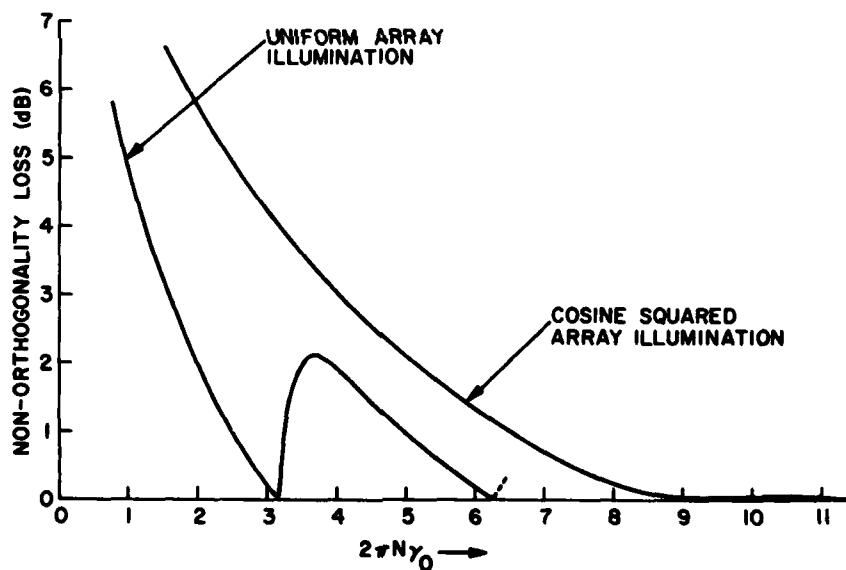


Figure 11. Non-Orthogonality Loss in the Feed for Uniform and Cosine Squared Illumination on Face B of the Feed Array

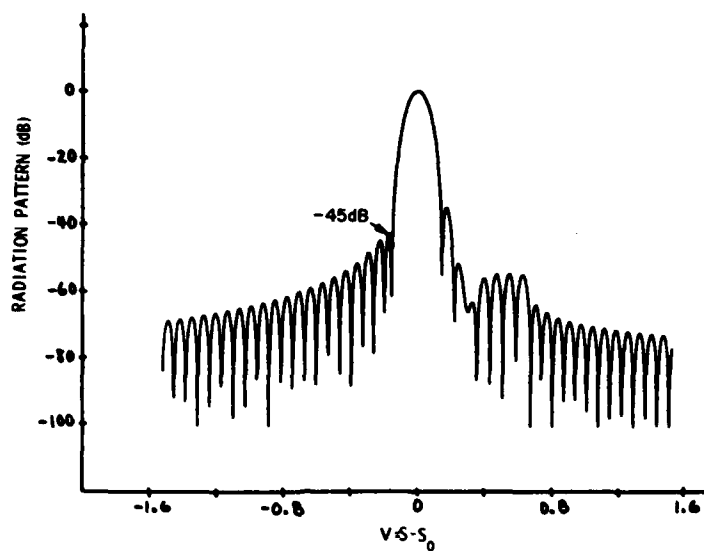


Figure 12. Radiation Pattern for  $2N = 2M = 16$ ,  $f = 16.4$ ,  $\gamma_0 = 0.0525$ ,  $S_0 = 1.5$  and  $f = 0.85 f_0$

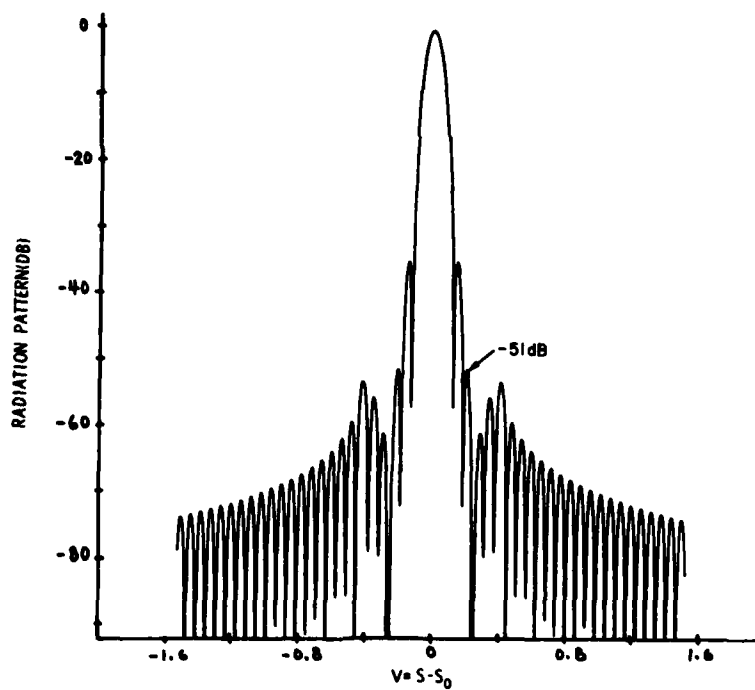


Figure 13. Radiation Pattern for  $2N = 2M = 16$ ,  $f = 16.4$ ,  $\gamma_0 = 0.0525$ ,  $S_0 = 1.5$  and  $f = f_0 (R = 1)$

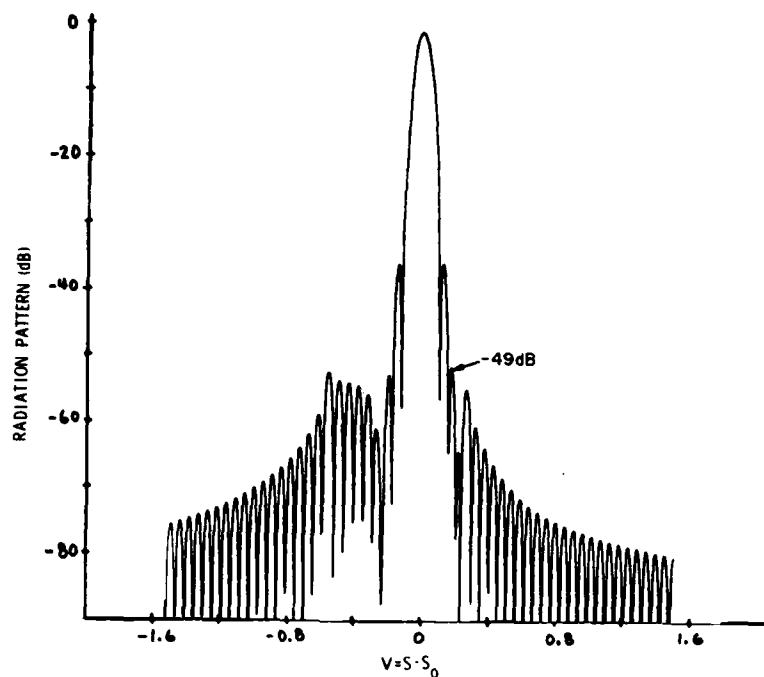


Figure 14. Radiation Pattern for  $2N = 2M = 16$ ,  $\gamma_0 = 0.0525$ ,  $l = 16.4$ ,  $S_0 = 1.5$  and  $f = 1.15 f_0$

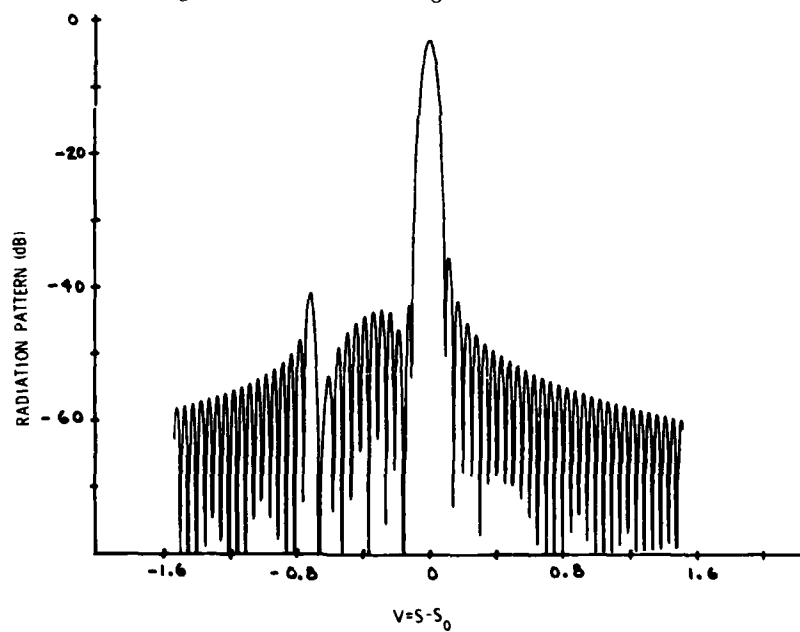


Figure 15. Radiation Pattern for  $l = 16.4$ ,  $2N = 2M = 16$ ,  $\gamma_0 = 0.0525$ ,  $S_0 = 15$ , and  $f = 1.25 f_0$

$R = f/f_0 = 0.85, 1.0, 1.15$  and  $1.25$ , respectively. From these figures we can see the effect of the sidelobes of the illumination on face B in Figure 1. For example, consider Figure 13. We note that the sidelobes begin dropping off in accordance with the distribution applied to the input parts (face A) but then rise again somewhat corresponding to diffraction sidelobes of the distribution,  $a_n$ , on face B.

From Figure 15 we also note that for  $R = f/f_0 = 1.25$  the grating lobe at  $S - S_0 \simeq -0.8$  begins appearing. At large values of  $R$  this grating lobe becomes even larger. This is in approximate agreement with (13) which predicts grating lobes for  $R \gtrsim (S_0 + 1)/(S_0 + \gamma) = (S_0 + 1)/(S_0 + N\gamma_0) = 1.29$ .

## 5. PHASE-ERROR SIDELOBES

Because, in addition to large bandwidth, we desire very low sidelobes. It is important to consider the effect on sidelobe level of random phase errors within the system. Let us assume that  $\sigma_A^2$  is the mean-square phase error at any of the input parts on face A,  $\sigma_B^2$  is the mean-square phase error (due to line-length errors, etc. in constructing the Rotman lens) on the elements of face B and  $\sigma_C^2$  is the mean-square phase error (due to line-length errors, etc.) on the planar (face C) of the lens. If these errors are small and uncorrelated, one from another, the mean relative sidelobe level produced by these errors is as shown in Appendix C

$$SL = \sigma_A^2 h_A(\theta) + \sigma_B^2 h_B(\theta) + \sigma_C^2 h_C \quad (24)$$

The quantities  $h_A$ ,  $h_B$ ,  $h_C$  are tabulated in Table 2, for parameters corresponding to the results shown in Figures 12 to 15. Note that  $h_A$  and  $h_B$  are functions of  $\theta$ , whereas, as expected,  $h_C$  is not. For the worst case (outside of the main beam) Eq. (24) can be approximated by

$$SL \simeq 0.11\sigma_A^2 + 0.0036\sigma_B^2 + 0.077\sigma_C^2 \quad (25)$$

We emphasize that (25) is a worst case result, and the coefficient of  $\sigma_A^2$  for large values of  $\theta$  will be much less than 0.11, as is evident from Table 2. From (25) we see that if we desire all sidelobes beyond the first to be smaller than -50 dB we require  $\sigma_A^2$ ,  $\sigma_B^2$  and  $\sigma_C^2$  be such that  $0.11\sigma_A^2 + 0.0036\sigma_B^2 + 0.077\sigma_C^2 \leq 10^{-5}$ .

Table 2. Error-Sidelobe Coefficients for  $2M = 2N = 16$ ,  
 $2K = 72$ ,  $\alpha = 1.833$ ,  $Q = 0.02164$ ,  $g = 0.05144$ ,  $\epsilon = 0.833$

$\sin \theta$	$h_A$	$h_B$	$h_C$
0.05	0.094	0.066	0.077
0.1	0.094	0.015	0.077
0.15	0.094	0.00067	0.077
0.175	0.093	0.0023	0.077
0.20	0.11	0.0036	0.077
0.225	0.039	0.0017	0.077
0.25	0.00030	0.00022	0.077
0.3	0.0004	0.0016	0.077
0.4	0.000081	0.00097	0.077
0.5	0.000037	0.00067	0.077
0.6	0.000023	0.00051	0.077
0.7	0.000017	0.00042	0.077
0.8	0.000014	0.00037	0.077

## 6. SUMMARY AND DISCUSSION

We have shown that it is possible to design an overlapped subarraying feed (scanned in one dimension) which has excellent sidelobe performance over a relatively wide bandwidth. The principal design parameters, once the number of beams (subarrays) is chosen, are  $\gamma_0 = \Delta D / \lambda_0 F$  and  $l = L/D$ . We have found that  $L$  should be chosen so that  $l$  is slightly larger than  $2M$ , where  $2M$  is the number of overlapped subarrays (beams). We suggest  $l = 1.025 (2M)$ . The parameter  $\gamma_0$  should be chosen as  $\gamma_0 = 0.85/(2N)$ .

In addition to the canonical 16 beam (subarray) system considered in this paper we have also studied eight and 32 beam systems. For the 32 beam system the results were much the same as presented here, but for the eight beam system we found it much more difficult to obtain the low sidelobe levels desired.

As discussed in Appendix A, we also considered the case in which the lens lies in the near field of the feed. The principal effect of including near-field effects appears to be a filling in of some of the pattern nulls, but with relatively little change in the sidelobe levels.

Finally, we should mention that there are numerous possible extensions of this study, such as: (1) Scanning in two dimensions rather than only one; (2) Use of a flat surface for the inner face of the lens rather than the cylindrical one we



considered; (3) The possibility suggested by Mailloux<sup>4</sup> of using nulls in  $a(\eta)$  to produce moveable nulls in the main beam of the radiation pattern. The possibility is evident from Eq. (9), because, in the absence of finite lens width effects, the radiation pattern is the product of the illumination on face B and the radiation pattern corresponding to the input distribution on the feed ports.

In Figures 16 to 18 we show, briefly, the effect of nulls in  $a(\eta)$  on the radiation pattern,  $F(S)$ . The simplest method of putting a null in  $F(S)$  is to place a null region in  $a(\eta)$ . According to (9), if  $a(\eta) = 0$  over the region  $\eta = \eta_0 - \delta/2$  to  $\eta = \eta_0 + \delta/2$ , then the radiation pattern  $F(S)$  should have a null in  $S$  space of width

$$W = \gamma\delta \quad (26)$$

centered, at midband, about  $S - S_0 = \gamma\eta_0$ . As before  $S = (D/\lambda_0) \sin \theta$  and  $S_0 = (D/\lambda_0) \sin \theta_0$ .

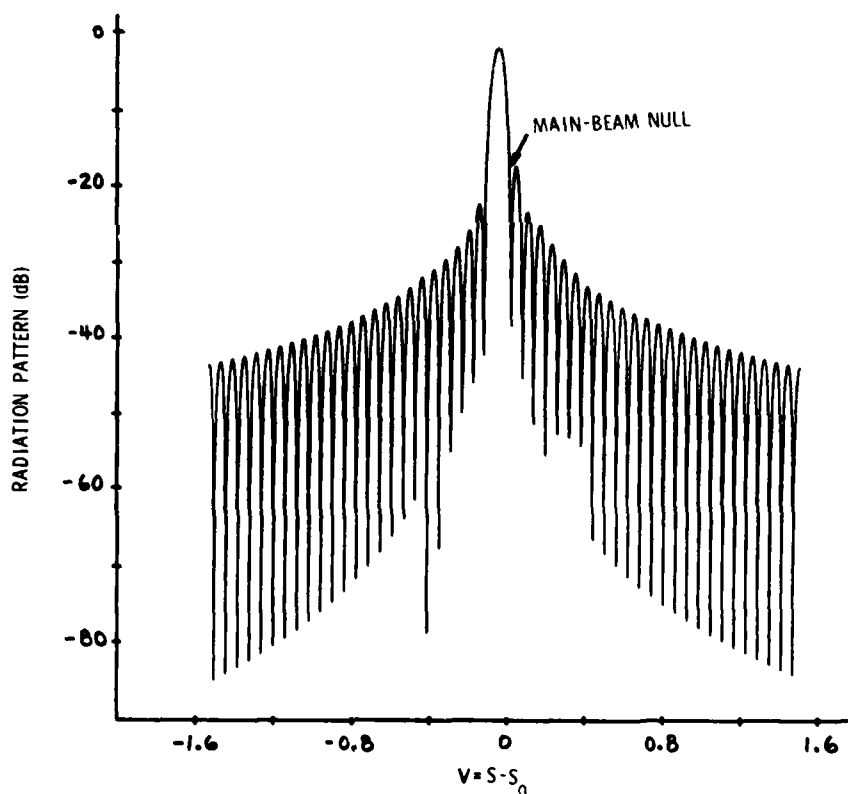


Figure 16. Main Beam Null Produced by Setting  $a_7 = a_8 = 0$  for  $2N = 2M = 16$ ,  $t = 16.4$ ,  $\gamma_0 = 0.0525$ ,  $S_0 = 1$  and  $R = 1$

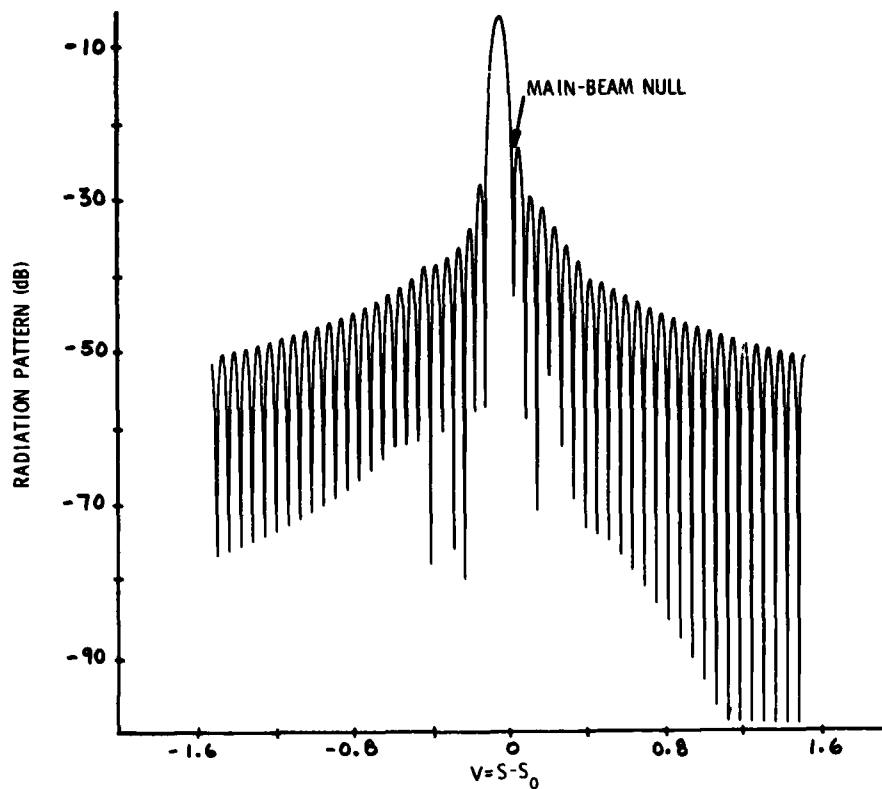


Figure 17. Main Beam Null Produced by Setting  $a_7 = a_8 = 0$ ,  $a_6 = a_9 = 0.5$ ,  $a_5 = a_{10} = 0.8$  and All Other  $a_n = 1$  for  $2N = 2M = 16$ ,  $l = 16.4$ ,  $\gamma_0 = 0.0525$ ,  $S_0 = 1.5$  and  $R = 1$

When the elements on face B of the feed array are discrete, as in Section 4 we replace  $\gamma$  by  $N\gamma_0$  and  $\delta$  by  $n_1/N$ , where  $n_1$  is the number of elements on face B with excitations,  $a_n$ , set equal to zero and  $\gamma_0$  was defined previously. Therefore, for a discrete feed, the width of the null in S space is

$$W = \gamma_0 n_1, \quad (27)$$

Eqs. (26) and (27) are ideal results; as we shall now see these null widths are not achieved in practice because of finite lens-width effects.

In Figure 16 we show the radiation pattern at midband when  $a_7 = a_8 = 0$ , but all the other fourteen elements on face B have  $a_n = 1$ . Upon comparing Figure 16 with Figure 13 we see that this results in a null which is -36 dB deep and located at  $S - S_0 = 0.034$ . Unfortunately, we obtain this null at the expense of much higher sidelobes. In particular, the second highest sidelobe is now -23 dB, as opposed to

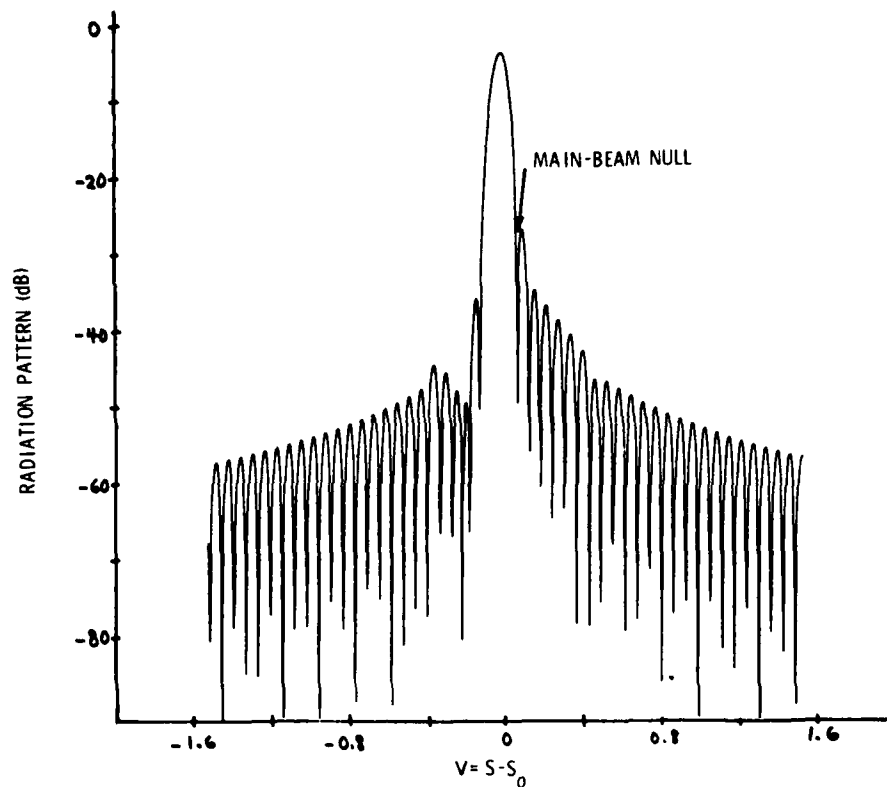


Figure 18. Main Beam Null Produced by Setting  $a_7 = a_8 = 0$ ,  $a_6 = a_9 = 0.5$ ,  $a_5 = a_{10} = 0.8$  and all Other  $a_n = 1$  for  $2N = 2M = 16$ ,  $S_0 = 1.5$ ,  $\gamma_0 = 0.0525$ ,  $l = 16.4$  and  $R = 0.975$

-51 dB for the case when all  $a_n = 1$ . We also note that the null is not nearly as wide as predicted by the ideal theoretical result in (27). In fact, using (27) gives a null width  $W = 2(0.0525) = 0.105$ , and this is very much greater than the actual null width in Figure 15. The cause of the higher sidelobes and partial null filling is, of course, the diffraction effects produced by the finite lens width,  $l$ .

The null width and sidelobe levels can be improved somewhat by tapering the excitations,  $a_n$ , rather than abruptly setting one or more  $a_n$  equal to zero. In Figure 17 we show the midband radiation pattern which results when  $a_7 = a_8 = 0$ ,  $a_6 = a_9 = 0.5$ ,  $a_5 = a_{10} = 0.8$  and all other  $a_n = 1$ . In this case there is a slight null broadening and about a 3 dB lowering of the sidelobes. Clearly, a further study of array illumination taper is required, but this will be deferred to a later paper.

Finally, we should comment on the bandwidth of the null. By using the ideal result in (9) we can readily show that the fractional null bandwidth is

$$FBW = \frac{S_o \gamma \delta}{S_o^2 - \left(\frac{\gamma \delta}{2}\right)^2} \quad (28)$$

The result in (28) gives the bandwidth over which a point target, located at the center of the null at midband, will remain within the null. For a discrete feed array, with the illumination,  $a_n$ , on  $n_1$  elements set equal to zero, (28) can be rewritten as

$$FBW = \frac{n_1 S_o \gamma_o}{S_o^2 - \left(\frac{n_1 \gamma_o}{2}\right)^2} \quad (29)$$

When the illumination,  $a_n$ , of two elements is set equal to zero,  $\gamma_o = 0.0525$  and  $S_o = 1.5$  the fractional null-bandwidth, as predicted by (29), is 0.14. This means that a target at null center at midband should remain with the null over a  $\pm 7$  percent frequency change. Unfortunately, because of finite lens-width effects, this also is very over-optimistic. In Figure 18 we show the radiation pattern for the system corresponding to that in Figure 17, but with  $R = f/f_o = 0.975$  instead of  $R = 1$ . We note that for  $R = 1$  the null was centered at  $S - S_o = 0.030$ , whereas for  $R = 0.975$  the null is centered at  $S - S_o = 0.069$ . (This shift does not occur when  $S_o = 0$ ). Furthermore, the null width is so small that the point  $S - S_o = 0.034$  is clearly not within the null. Therefore the realistic bandwidth is much less than  $\pm 2.5$  percent, rather than the ideal result of  $\pm 7$  percent. Again the problem is caused by the finite lens size,  $L$ .

It is evident from the brief discussion above that although this system exhibits some potential for placing moveable nulls in the main beam, further work will be required to determine how large  $L$  and  $N$  must be, and what distributions of illumination coefficients  $a_n$  will be required, in order to achieve nearly ideal null widths, null bandwidths and low sidelobes.

## References

1. Rudge, A. and Whithers, M. (1971) Proceedings of the IEE (UK) 118:857-863.
2. Tang, R. (1972) Proceedings of 1970 Phased Array Antenna Symposium Artech House, pp 254-260.
3. Borgiotti, G. (1977) IEEE Transcript on Antennas & Propagation, AP-25: 232-243.
4. Mailloux, R. (1979) Digest of 1979 IEEE International Antennas and Propagation Symposium, Seattle, Washington, pp 30-33.

## Appendix A

### Analysis of the General System

Here we shall analyze the general case when the lens (face C) is discrete, and lies in the near field of the feed system. In the near zone the field radiated by the feed when only the  $p^{\text{th}}$  port is excited is

$$f_p(u) = \sum_{n=-N+1}^N \frac{|a_n| \hat{g}_n(u)}{\rho_n^{1/2}} \exp \{-ik\rho_n + i\psi_n - iky_n u_p\} \quad , \quad (A1)$$

where

$$\rho_n = [F^2 - 2uFy_n + y_n^2]^{1/2} \quad ,$$

$u = \sin \phi$ ,  $y_n = (n - 1/2)\Delta$ ,  $\Delta$  is the separation between the radiating elements on face B of the feed,  $\hat{g}_n(u)$  is the radiation pattern on the  $n^{\text{th}}$  element and  $\psi_n$  is the phase of  $a_n$ . In writing (A1) it is implicitly assumed that  $\rho_n \gg \lambda_0$ .

Let us now expand  $\rho_n$  in a Taylor series about  $y_n = 0$ , and then retain only up to quadratic terms. The result is

$$f_p(u) = F^{-1/2} \sum_{n=-N+1}^N |a_n| \hat{g}_n(u) \exp \left\{ -ikF + iky_n u - i \frac{k}{2} \frac{y_n^2}{F} (1 - u^2) + i\psi_n - iky_n u_p \right\} . \quad (A2)$$

We can partially correct for the quadratic phase error in (A2) if we choose  $\psi_n = ky_n^2/2F$ . Then (A2) becomes

$$f_p(u) = F^{-1/2} e^{-ikF} \sum_{n=-N+1}^N |a_n| \hat{g}_n(u) \exp \left\{ iky_n(u - u_p) + \frac{iky_n^2 u^2}{2F} \right\} . \quad (A3)$$

From (A3) it is clear that (A3) can be approximated by (18) if  $ky_n^2 u^2/2F \ll 1$ . Upon recalling that the maximum value of  $Y_n$  is  $(N - 1/2)\Delta$  and that the maximum value of  $u$  is  $u = \sin \phi$ , where  $\phi_0$  is the angle subtended by the lens edge, we may rewrite this condition as

$$\frac{\pi(N - 1/2)\Delta^2}{\lambda F} \sin^2 \phi_0 < 1 . \quad (A4)$$

We now assume that (A4) does not necessarily hold, but that the fixed time correction  $\psi_n = ky_n^2/2F$  is applied to the feed, so that (A1) is the field incident on the inner face of the lens. The lens is assumed to consist of  $2K$  discrete probes which are separated by a distance  $\epsilon\lambda_0/2$ , where  $0 \leq \epsilon \leq 1$ , on the flat face of the lens (plane) (in Figure 1). When  $I_p$  is given by (20), we obtain the radiated field

$$F(\theta) = \sum_{t=1}^{2K} \sum_{n=1}^{2N} a_{n-N-1/2} \hat{g}_{n-N-1/2} \left( \frac{v_t}{2} \right) \rho_{nt}^{-1/2} \frac{\sin M\Phi_n}{2M \sin(\Phi_n/2)} \frac{\cos \Phi_n \left[ 1 - \cos \frac{\pi}{M} \right]}{\cos \Phi_n - \cos \left( \frac{\pi}{M} \right)} \exp \left\{ \frac{i\pi}{g} \left[ Rh_n^2 - 2R\rho_{nt} + v_t(R \sin \theta - \sin \theta_0) \right] \right\} \quad (A5)$$

where  $R = \lambda_0/\lambda$ ,  $g = \lambda_0/F$ ,  $v_t = \epsilon g(t - K - 1/2)$ ,  $h_n = Q(n - N - 1/2)$ ,  $Q = \Delta/F$ ,  $\rho_{nt} = (1 - v_t h_n + h_n^2)^{1/2}$ ,  $\Phi_n = 2\pi[(R - 1)\alpha \sin \theta_0 + \alpha R h_n]$ , and  $\alpha = D/\lambda_0$ , where  $D$  is the subarray spacing on face C.

If all the feed elements on face B are uniformly weighted, so that  $a_n = 1$ , and their element patterns are isotropic we can simplify (A5) to

$$F(\theta) = \sum_{n=1}^{2N} \sum_{t=1}^{2K} \rho_{nt}^{-1/2} \frac{\sin M\phi_n}{2M \sin\left(\frac{\phi_n}{2}\right)} \cdot \frac{\cos \phi_n \left[1 - \cos \frac{\pi}{M}\right]}{\cos \phi_n - \cos\left(\frac{\pi}{M}\right)} \cdot \exp \left\{ i \frac{\pi R}{g} \left[ h_n^2 - 2\rho_{nt} + v_t (\sin \theta - R^{-1} \sin \theta_0) \right] \right\} \quad (A6)$$

Eq. (A6) has been evaluated for a case corresponding to the results shown in Figures 12 to 15. If we choose  $2M = 2N = 16$ ,  $L = 30\lambda_0$  and  $t = L/D = 16.4$  then  $\alpha \equiv D/\lambda_0 = 1.833$ . Also, because  $\gamma_0 = \Delta D/\lambda_0 F = \alpha Q = 0.0525$  then we automatically have  $Q = 0.0525/\alpha = 0.02864$ . Next,  $g$  is chosen so that the outermost feed beam has its center at  $\phi = \pi/4$ . This gives  $g = \lambda_0/F = 0.05144$ . Finally, in Figures 12 to 15,  $S_0 = (D/\lambda_0) \sin \theta_0 = \alpha \sin \theta_0 = 1.5$ . Therefore  $\sin \theta_0 = 0.818$  and the scan angle,  $\theta_0$ , is equal to  $55^\circ$ . The results of this exact calculation are shown in Figures 19 to 21. Observe that the sidelobe levels do not differ significantly from those obtained using the approximate result in (21). The principal effect is the filling in of some of the nulls because of the uncorrected quadratic errors in (A1).

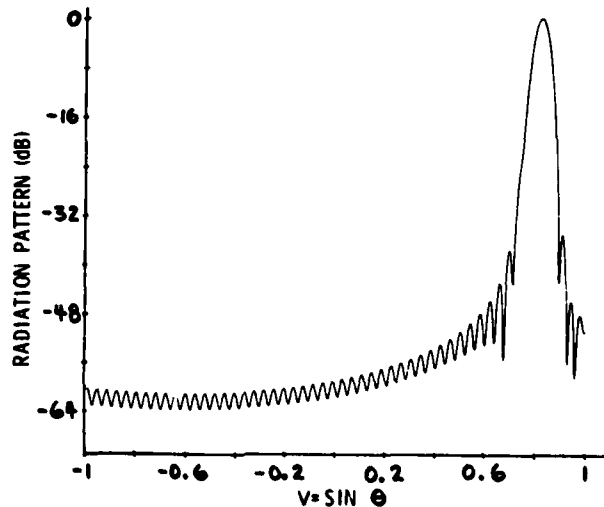


Figure 19. Radiation Pattern Including Discrete Lens and Near-Field Effects for  $2N = 2M = 16$ ,  $\alpha = 1.833$ ,  $Q = 0.02864$ ,  $g = 0.05144$  and  $R = 0.85$



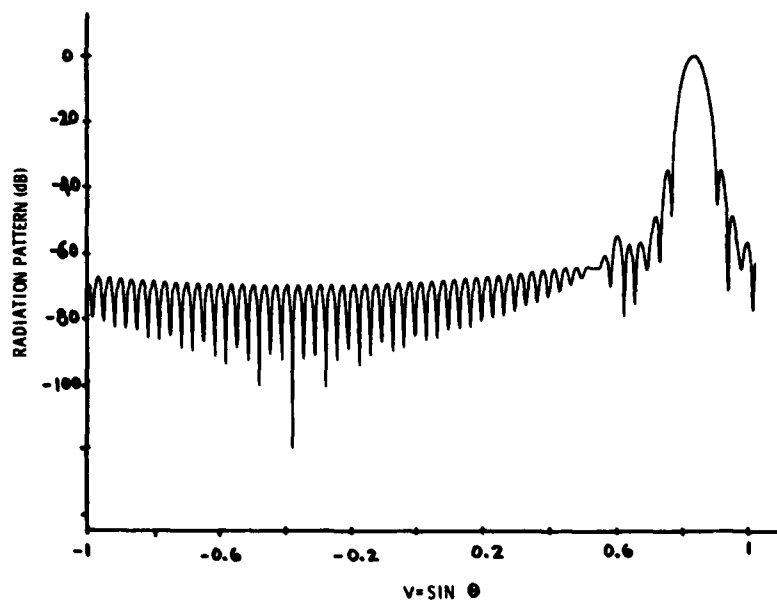


Figure 20. Radiation Pattern Including Discrete Lens and Near-Field Effects for  $2N = 2M = 16$ ,  $\alpha = 1.833$ ,  $Q = 0.02864$  and  $R = 1$

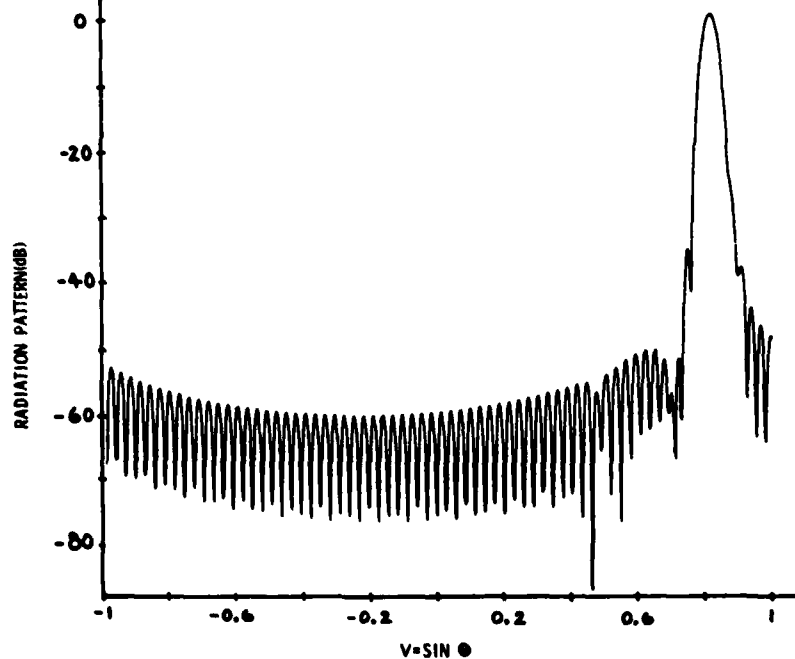


Figure 21. Radiation Pattern Including Discrete Lens and Near-Field Effects for  $2N = 2M = 16$ ,  $\alpha = 1.833$ ,  $Q = 0.02864$ ,  $g = 0.05144$ , and  $R = 1.15$

## Appendix B

### Effect of Subarray Non-Orthogonality

In order to consider the orthogonality properties of the subarray beams, let us consider the integral:

$$J_{pq} = \int_{-1}^1 du f_p(u) f_q^*(u) , \quad (B1)$$

where  $f_p(u)$  is the pattern of the  $p^{\text{th}}$  subarray beam. The  $p^{\text{th}}$  and  $q^{\text{th}}$  beams are orthogonal if  $J_{pq} = 0$  for  $p \neq q$ . Let us now substitute (17) into (B1). We obtain

$$J_{pq} = 2 \sum_{n=-N+1}^N \sum_{m=-N+1}^N a_n a_m^* \exp \left\{ -i \frac{2\pi\Delta}{\lambda_0} R [(n - 1/2) u_p - (m - 1/2) u_q] \right\} \\ \cdot \text{sinc} \left[ \frac{2\pi\Delta R}{\lambda_0} (n - m) \right] , \quad (B2)$$

where  $u_p = (p - 1/2) \beta D / F$ ,  $\text{sinc } t = \sin t / t$  and  $R = \lambda_0 / \lambda$ . In order to study  $J_{pq}$  let us assume  $R = 1$ , and  $\Delta = \lambda_0 / 2$ . Then because  $\text{sinc } \pi (n - m) = 0$  unless  $n = m$  (B2) becomes

$$J_{pq} = 2 \sum_{n=-N+1}^N |a_n|^2 \exp[-i\pi(n - 1/2)(u_p - u_q)] \quad (B3)$$

For the case when face B (in Figure 1) has the uniform weighting,  $|a_n| = 1$ , we get:

$$J_{pq} = \frac{2 \sin \left[ \frac{N\pi D}{F} (p - q) \right]}{\sin \left[ \frac{\pi D}{2F} (p - q) \right]} \quad (B4)$$

From (B4) it is readily seen that  $J_{pq} = 0$  for  $p \neq q$  only if

$$\frac{ND}{F} = \pm n ,$$

where  $n = 1, 2, 3, \dots$ . Therefore, the beams are orthogonal when  $\lambda_o = 2\Delta$  only if  $N$ ,  $D$ , and  $F$  are chosen so that (B5) holds. The beams are not orthogonal when  $\lambda \neq \lambda_o$  even if (B5) is satisfied.

When the beams are non-orthogonal, there is a system loss due to reflection at the input ports (even if the Butler matrix or Rotman lens is lossless). Stein,<sup>B-1</sup> has presented a theory for estimating this loss. He shows that the maximum radiation efficiency is given by

$$\eta = \frac{1}{\beta_{\max}} \quad (B6)$$

where  $\beta_{\max}$  is the largest eigenvalue of the matrix  $[R_{pq}]$  where

$$R_{pq} = \frac{J_{pq}}{J_{pp}} \quad (B7)$$

and  $J_{pq}$  is given by (B2). We have evaluated the maximum efficiency for the case when  $\Delta = \lambda_o/2$  as the parameter

$$2\pi N\gamma_o = \frac{2\pi N\Delta D}{\lambda_o F}$$

B-1. Stein, S. (1962) IRE Transcript on Antennas & Propagation, AP-10:548-557.

is varied. The results are presented in Figure 11 for the cases when  $a_n = 1$  and  $|a_n| = 1$  and  $|a_n| = \cos^2 \pi(n - N - 1/2)/2N$ . We note that, as expected, the orthogonality loss for the uniform illumination is zero when the beams are mutually orthogonal; this occurs when  $2\pi N\gamma_0 = \pi, 2\pi, 3\pi$ , etc. However, for  $2N\gamma_0 \ll 1$  we see that there is considerable reflection loss because of non-orthogonality. This conclusion holds for both the uniform and cosine square taper on face B. This figure also shows that for a system with  $2N\gamma_0 \simeq 1$  there is a 4 dB reflection loss penalty paid by using a cosine squared array illumination as opposed to a uniform weighting on face B of the feed. Therefore, unless the cosine squared illumination gives considerably better sidelobe behavior in  $F(S)$ , it is not a desirable weighting.

## Appendix C

### Sidelobes Due to Phase Errors

Here we shall assess the effect of phase errors on the radiation pattern of the system. Let us suppose that  $\psi_A(p)$  is the phase error on the input to the  $p^{\text{th}}$  port on face A of the feed,  $\psi_B(n)$  is the phase error (due to line-length errors, etc. in the feed lens) of the  $n^{\text{th}}$  element on face B of the feed and  $\psi_C(t)$  is the phase error on the  $t^{\text{th}}$  radiating element at face C of the feed due to line-length errors, etc. in constructing the lens. We shall assume that these phase errors are all random and uncorrelated, and that

$$\langle \psi_A(p) \rangle = \langle \psi_B(n) \rangle = \langle \psi_C(t) \rangle = 0 \quad , \quad (C1)$$

$$\langle \psi_A(p) \psi_A(p') \rangle = \sigma_A^2 \delta_{pp'} \quad , \quad (C2)$$

$$\langle \psi_B(n) \psi_B(n') \rangle = \sigma_B^2 \delta_{nn'} \quad , \quad (C3)$$

$$\langle \psi_C(t) \psi_C(t') \rangle = \sigma_C^2 \delta_{tt'} \quad , \quad (C4)$$

where  $\delta_{pp'}$  is the Kronecker delta and  $\langle \rangle$  denotes an ensemble average. Thus we have assumed that the phase fluctuations are completely uncorrelated from element to element (and, of course, from face to face).

When the phase errors are included we find that, for uniform excitation on face B ( $a_n = 1$ ) the field distribution at position  $x_t$  on face C of the lens is given by

$$f(x_t) = \sum_{p=-M+1}^M \hat{I}_p \sum_{n=-N+1}^N \exp \left\{ i\psi_A(p) - i2\pi(p - 1/2)(R - 1) S_0 + i\psi_B(n) + iky_n \left( \frac{x_t}{F} - u_p \right) \right\} \quad (C5)$$

where  $u_p = (p - 1/2)D/F$  and  $y_n = (n - 1/2)\Delta$ , and  $D$ ,  $F$  and  $\Delta$  were defined previously. In writing (C5) we have implicitly assumed that the lens is in the far field of the feed, so that the term  $ky_n^2 u^2 / 2F$  in (A3) is negligible. For simplicity we shall also assume that the beam is scanned to  $\theta_0 = 0$  so that  $S_0 = 0$ . Then (C5) becomes

$$f(x_t) = \sum_{p=-M+1}^M \sum_{n=-N+1}^N \hat{I}_p \exp \left\{ i\psi_A(p) + i\psi_B(n) + iky_n \left( \frac{x_t}{F} - u_p \right) \right\} \quad (C6)$$

The aperture distribution in (C6) produces a radiation pattern

$$F(\theta) = \sum_{t=-K+1}^K \sum_{p=-M+1}^M \sum_{n=-N+1}^N \hat{I}_p \exp \left\{ ik \left( x_t \sin \theta + \frac{y_n x_t}{F} - y_n u_p \right) + i\psi_A(p) + i\psi_B(n) + i\psi_C(t) \right\} \quad (C7)$$

where  $x_t = (t - 1/2)\epsilon\lambda_0/2$  is the location of the  $t^{\text{th}}$  radiator on face C of the lens. The ensemble averaged radiation pattern can be obtained by taking the ensemble average of  $FF^*$ , and then using the fact that  $\psi_A$ ,  $\psi_B$  and  $\psi_C$  are uncorrelated. This gives

$$\begin{aligned} \langle |F|^2 \rangle &= \sum_t \sum_{t'} \sum_p \sum_{p'} \sum_n \sum_{n'} \hat{I}_p \hat{I}_{p'}^* \exp \{ ik[\rho(t, n, p) - \rho(t', n', p')] \} \\ &\quad \cdot \langle \exp[i\psi_A(p) - i\psi_A(p')] \rangle \langle \exp[i\psi_B(n) - i\psi_B(n')] \rangle \\ &\quad \cdot \langle \exp[i\psi_C(t) - i\psi_C(t')] \rangle \quad (C8) \end{aligned}$$

where

$$\rho(t, n, p) = x_t \sin \theta + \frac{x_t y_n}{F} - y_n u_p \quad (C9)$$

We next assume all phase errors are small compared with unity, then expand the exponentials in (C8) in a Taylor series and finally apply (C1) (C4). The result is

$$\begin{aligned} \langle |F|^2 \rangle &= (1 - \sigma_A^2)(1 - \sigma_B^2)(1 - \sigma_C^2) \left| \sum_t \sum_n \sum_p \hat{I}_p e^{ik\rho(t, n, p)} \right|^2 \\ &+ \sigma_A^2 \sum_p |\hat{I}_p|^2 \left| \sum_n \sum_t e^{ik\rho(t, n, p)} \right|^2 + \sigma_B^2 \sum_n \left| \sum_p \sum_t \hat{I}_p e^{ik\rho(t, n, p)} \right|^2 \\ &+ \sigma_C^2 \sum_t \left| \sum_p \sum_n \hat{I}_p e^{ik\mu(t, n, p)} \right|^2 \end{aligned} \quad (C10)$$

where

$$\mu(t, n, p) = \frac{y_n x_t}{F} - y_n u_p$$

Because the mean square phase errors are small we can neglect  $\sigma_A^2$ ,  $\sigma_B^2$  and  $\sigma_C^2$  compared with unity in the first term in (C10). Also, upon remembering the relative sidelobe level due to phase errors is

$$SL = SL_A + SL_B + SL_C \quad (C11)$$

where

$$SL_A = \frac{\sigma_A^2}{F_o} \sum_p |\hat{I}_p|^2 \left| \sum_t \sum_n e^{ik\rho(t, n, p)} \right|^2 \quad (C12)$$

$$SL_B = \frac{\sigma_B^2}{F_o} \sum_n \left| \sum_p \sum_t \hat{I}_p e^{ik\rho(t, n, p)} \right|^2 \quad (C13)$$

$$SL_C = \frac{\sigma_C^2}{F_o} \sum_t \left| \sum_p \sum_n \hat{I}_p e^{ik\mu(t, n, p)} \right|^2 \quad (C14)$$

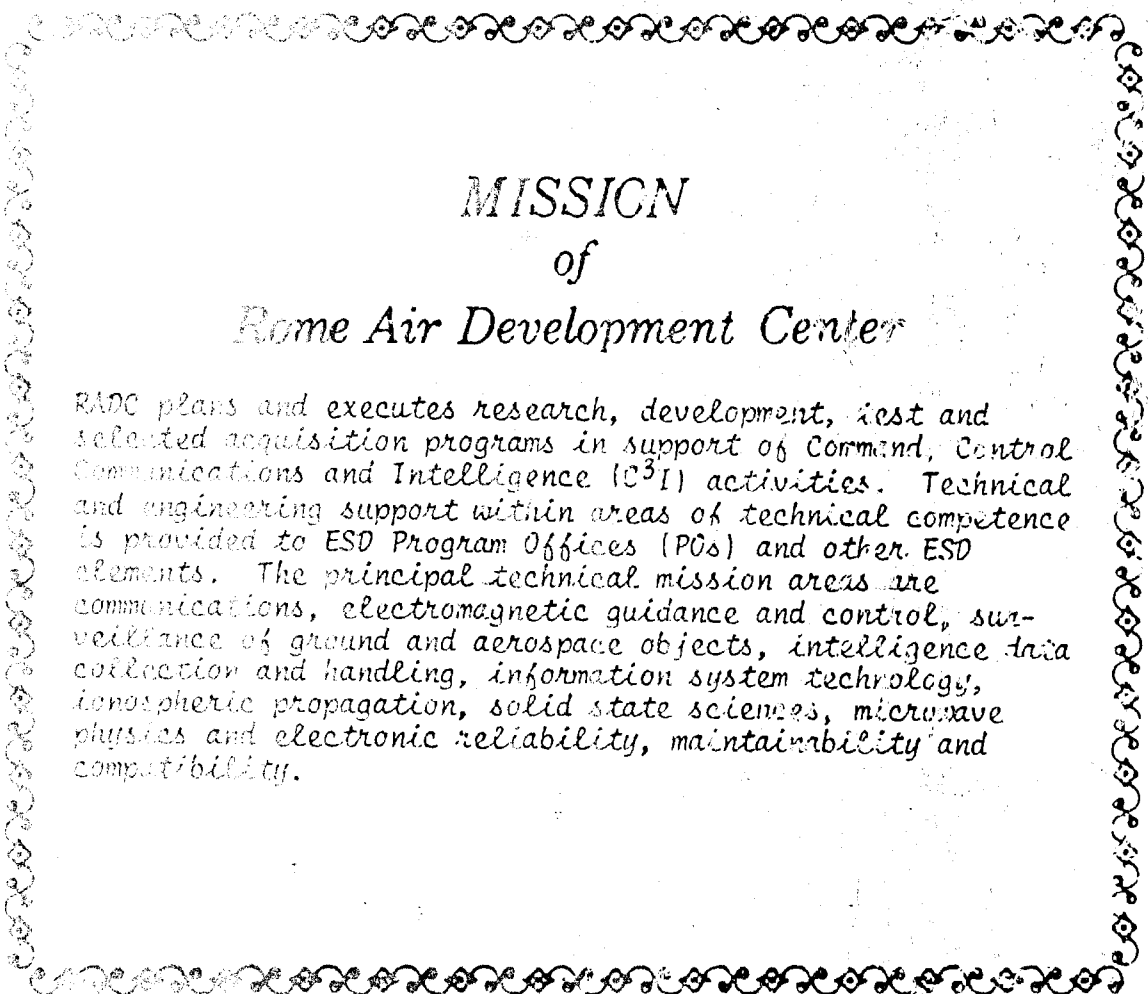
$$F_o = \left| \sum_t \sum_n \sum_p \hat{f}_p e^{ik\mu(t, n, p)} \right|^2 \quad (C15)$$

The relative sidelobe levels have been numerically evaluated for the case when  $\epsilon = 0.833$ ,  $2K = 72$ ,  $\alpha = D/\lambda_o = 1.833$ ,  $Q = \Delta/F = 0.02864$ , etc. (the same conditions as in Appendix A). The result obtained is

$$SL = \sigma_A^2 h_A(\theta) + \sigma_B^2 h_B(\theta) + \sigma_C^2 h_C \quad (C16)$$

where  $h_A$ ,  $h_B$  and  $h_C$  are given in Table 2.





## *MISSION of Rome Air Development Center*

RADC plans and executes research, development, test and selected acquisition programs in support of Command, Control Communications and Intelligence (C<sup>3</sup>I) activities. Technical and engineering support within areas of technical competence is provided to ESD Program Offices (POs) and other ESD elements. The principal technical mission areas are communications, electromagnetic guidance and control, surveillance of ground and aerospace objects, intelligence data collection and handling, information system technology, ionospheric propagation, solid state sciences, microwave physics and electronic reliability, maintainability and compatibility.